

# Percolation effect of V<sub>2</sub>O<sub>5</sub> nanorod/graphene oxide nanocomposite films for stable fast-switching electrochromic performances



Bon-Ryul Koo<sup>a</sup>, Ju-Won Bae<sup>b</sup>, Hyo-Jin Ahn<sup>a,b,\*</sup>

<sup>a</sup> Program of Materials Science & Engineering, Convergence Institute of Biomedical Engineering and Biomaterials, Seoul National University of Science and Technology, Seoul, 01811, South Korea

<sup>b</sup> Department of Materials Science & Engineering, Seoul National University of Science and Technology, Seoul, 01811, South Korea

## ARTICLE INFO

### Keywords:

Films  
Electrical properties  
Optical properties  
Carbon  
Electrochromic performances

## ABSTRACT

In the present study, V<sub>2</sub>O<sub>5</sub> nanorod (VR)/graphene oxide (GO) nanocomposite films that can be used as an electrochromic (EC) material have been developed using the sol-gel spin-coating method. In order to optimize the nanocomposite effect of GO consisting of the VR films on EC performances, we controlled the volume percentage of GO compared to vanadium precursor to 0, 1, 2, and 3 vol%. With the increase of GO in VR films to 2 vol%, the resultant films exhibited a densely percolated structure, which was due to the nanocomposite effect of GO to generate the VR growth by an interaction with the oxygen-containing functional groups of GO. Due to the effect of optimized GO, the VR/GO nanocomposite films fabricated with 2 vol% GO revealed fast switching speeds (2.5 s for the bleaching speed and 1.4 s for the colouration speed). This was the result of an improved electrical conductivity and ion diffusion coefficient and high cycling retention of transmittance modulation (94.90% after 500 cycles) stemming from the remarkable electrochemical stability of the films as compared to those of bare VR films.

## 1. Introduction

With the ever-increasing development of various optoelectronic devices, such as automobile sunroofs and mirrors, electronic displays, and smart windows, electrochromic devices (ECDs) have attracted an enormous interest. ECDs have unique properties of reversibly changing the optical properties (colour, reflection, and transmittance) as the result of applied voltage [1–4]. A complementary ECD has a sandwich-like structure with five functionalized layers of cathodic and anodic electrochromic (EC) layers, two transparent conducting layers, and an electrolyte layer. The practical use of the ECDs requires considering several aspects of their performance, such as transmittance modulation, switching speed, colouration efficiency (CE), and cycling retention [5]. The current limitations in these parameters make it imperative to develop unique EC materials being in charge of reaction capacity and kinetics during electrochemical behaviour. Among a variety of EC materials developed thus far, vanadium oxide (V<sub>2</sub>O<sub>5</sub>) has been reported to be a promising material. Vanadium oxide has exceptional EC characteristics that implement multicolour variation (blue-green-yellow) by reversible ion insertion/extraction processes and use both anodic and cathodic materials in the ECDs [6]. However, since V<sub>2</sub>O<sub>5</sub> has low electrical conductivity and ion diffusion coefficient, which could

degrade the EC performances, its practical use as a EC material in practical industrial applications remains limited [7,8]. Effective ways to improve the EC performances using V<sub>2</sub>O<sub>5</sub> include nanostructuring of the films to a short transport distance of ions and electrons and providing abundant electroactive sites during the electrochemical reaction, such as nanorod, nanowire, and nanobelts [9–11]. In addition, another effective way to increase the electrical conductivity and relax the volume expansion of V<sub>2</sub>O<sub>5</sub> during EC reactions is creating the nanocomposite of V<sub>2</sub>O<sub>5</sub> with other materials (MoO<sub>3</sub>, NiO, and TiO<sub>2</sub>) so that to accelerate the electrochemical reaction, which results in an improvement of the switching speed and the cycling retention of the ECDs [12–14]. However, although these efforts have been applied by many research terms, none of these studies has reported the precise process of nanostructuring V<sub>2</sub>O<sub>5</sub> films using GO for high-performance ECDs.

In the present study, we developed VR/GO nanocomposite films using the sol-gel spin coating method. Nanocomposite of GO offer the VR film several benefits, thereby enhancing electrical conductivity and electrochemical stability by forming the interconnected network as a backbone, thus forming a percolated film structure to improve EC performances. In addition, we also optimized the amount of GO to form high-performance VR/GO nanocomposite films by proving the relationship between their morphological, structural, chemical, and

\* Corresponding author. Department of Materials Science & Engineering, Seoul National University of Science and Technology, Seoul, 01811, South Korea.  
E-mail address: [hjahn@seoultech.ac.kr](mailto:hjahn@seoultech.ac.kr) (H.-J. Ahn).

<https://doi.org/10.1016/j.ceramint.2019.03.148>

Received 15 February 2019; Received in revised form 12 March 2019; Accepted 20 March 2019

Available online 23 March 2019

0272-8842/ © 2019 Elsevier Ltd and Techna Group S.r.l. All rights reserved.

optoelectronic properties and EC performances.

## 2. Experimental

The VR/GO nanocomposite films were fabricated using the sol-gel spin-coating method. First, the sol-gel solutions for spin coating were prepared by dissolving 0.1 M vanadium oxide ( $V_2O_5$ , Alfa Aesar) as a vanadium precursor and 10 wt% polyvinylpyrrolidone (PVP,  $M_w = 1,300,000$  g/mol, Aldrich) as an adhesion agent into a mixture consisting of 95 vol% de-ionized (DI) water and 5 vol% hydrogen peroxide ( $H_2O_2$ , Junsei). After stirring, the obtained solutions were mixed with the GO (MExplorer), where the volume percentage of the added GO in comparison with vanadium precursor varied (0, 1, 2, and 3 vol%) to optimize the percolation effect of the GO on the VR films. The resultant solutions were spin-coated on the FTO glass substrates (Pilkington,  $8.0 \Omega/\square$ ) at the spin speed of 2000 rpm for 30 s, which were annealed at 500 °C for 1 h under the air atmosphere, which resulted in obtaining four types of the VR/GO nanocomposite films with 0, 1, 2, and 3 vol% GO (hereafter referred to as bare VR, VR/G1, VR/G2, and VR/G3, respectively).

The morphological and topographical properties of the films were characterized using field-emission scanning electron microscopy (FESEM, Hitachi S-4800) and atomic force microscopy (AFM, diDimension™ 3100), respectively. The structural characterization of the films was investigated by X-ray diffraction (XRD, Rigaku D/MAX2500V). The chemical binding states were analysed using X-ray photoelectron spectroscopy (XPS, AXIS ultra-delay line detector equipped with an Al  $K_{\alpha}$  X-ray source, KBSI Daedeok Headquarters). The bonding structure of GO was characterized by a Raman spectrometer (JASCO NRS-5100) using the laser-excitation wavelength of 532.1 nm. The electrical and optical properties were measured by a Hall-effect measurement (Ecopia, HMS-3000) and an ultraviolet-visible (UV-vis) spectroscopy (Perkin-Elmer, Lambda-35), respectively. The measurement of electrochemical and EC performances was performed in a three-electrode electrochemical cell composed with 1 M  $LiClO_4$  ( $\geq 95.0\%$ , Aldrich) in propylene carbonate (anhydrous, 99.7%, Aldrich) as the electrolyte, Pt wire as the counter electrode, and Ag wire as the reference electrode using a potentiostat/galvanostat (PGSTAT302N, FRA32M, Metrohm Autolab B.V., the Netherlands). The tracing of *in-situ* optical properties was performed by ultraviolet-visible (UV-vis) spectroscopy (Perkin-Elmer, Lambda-35) at the wavelength at 415 nm.

## 3. Results and discussion

Fig. 1 shows top-view FESEM images of (a) bare VR, (b) VR/G1, (c) VR/G2, and (d) VR/G3, respectively. Bare VR reveals a rough film structure with vacant gaps between nanorod-shaped crystallites cross-linked together. With an increase of the amount of the GO for forming the films to 3 vol%, the film structures gradually become more dense, which can be attributed to the nanocomposite effect of the GO acting as reactive sites for the growth of the VR induced by the interaction with their oxygen-containing functional groups, resulting thus in the formation of a densely percolated film structure [15]. In addition, there is a moderate decrease of the nanorod-shaped crystallite size from 92.5–242.3 nm (avg. 160.0 nm) for bare VR to 59.5–226.2 nm (avg. 123.5 nm) for VR/G3, which is another piece of evidence of the accelerating percolation effect of the film structure [16]. The realization of the densely percolated film structure is also confirmed by the TEM results of VR/G2 peeled off from FTO glass substrate (see Fig. 1(e) and (f)). It can be seen that the GO matrix was combined with nanorod-shaped crystallites crosslinked together. In addition, the enlarged TEM image further demonstrates that the crystallite with well-defined lattice spacing of ca. 0.43 nm, corresponding to the (001) interplane of orthorhombic  $V_2O_5$ , was perfectly covered with the GO matrix [17]. This can imply that oxygen-containing functional groups of the GO interact

with the VR to form a strong linking between them, which is beneficial to the short ions diffusion path on the VR and prevents variation of  $V_2O_5$  lattice during the EC reactions [18,19]. In the AFM results shown in Fig. 2, by performing nanocomposite of the GO with thickness of 4.81–5.28 nm (see Fig. 2a and S1a), the decrease in root-mean-square roughness ( $R_{ms}$ ) of VR/G2 (22.2 nm, see Fig. 2c and S1c) as compared to bare VR (30.6 nm, see Fig. 2b and S1b) was clearly observed, which is due to the formation of the densely percolated film structure. Therefore, due to the high electrical conductivity and mechanical strength of the films, the nanocomposite of the GO for forming the VR films can be useful to ion transport and cycling retention of the films during the EC reaction [20].

Fig. 3a shows the XRD patterns obtained from bare VR, VR/G1, VR/G2, and VR/G3. All films reveal equally characteristic diffraction peaks emitted at 20.2°, which corresponds to the (001) plane, of orthorhombic  $V_2O_5$  (JCPDS No. 89–0612). The emitted peak of the films was broadened with an increase of the volume percentage of the GO used in preparation of the films (see Fig. S2a). This suggests that the grain size of the  $V_2O_5$  gradually decreased. This is evident when looking at the values in the grain size of all films (26.5 nm for bare VR, 24.4 nm for VR/G1, 21.7 nm for VR/G2, and 19.0 nm for VR/G3 for bare VR) calculated by the Bragg's equation ( $n\lambda = 2d\sin\theta$ ), which is consistent with the SEM results. However, due to the relatively small amount of the GO as compared to  $V_2O_5$ , the peaks related to the GO cannot be identified in the XRD results. To characterize the existence of the GO in the films, we performed the Raman analysis (Fig. 3b). Compared to bare VR, the films with the GO exhibited both G band ( $1591.3 \text{ cm}^{-1}$ ,  $E_{2g}$  phonon of  $C sp^2$  atoms) and D band ( $1365.6 \text{ cm}^{-1}$ ,  $\kappa$ -point phonons of  $A_{1g}$  symmetry); this finding is consistent with the results reported by Li et al. and Sen et al. [16,21]. Specifically, the intensity of these bands increased from VR/G1 to VR/G3, which is a major evidence of an increasing amount of the GO with the  $sp^2$  domains in the films [16]. In addition, we used the XPS analysis to analyse the chemical states of the films by the nanocomposite of the GO with the  $V_2O_5$ . All binding energies were calibrated by C 1s (284.5 eV) as reference. In the XPS V  $2p_{3/2}$  spectra (see Fig. 3c), characteristic peaks of the films were equally emitted at 516.9 and 515.3 eV, indicating the binding energy of  $V^{5+}$  and  $V^{4+}$ , respectively, related to the  $V_2O_5$  phase [6]. From XPS C 1s spectra (see Fig. 3d), two characteristic peaks of C-C (284.5 eV) and C-OH (286.2 eV) were observed; interestingly, there was a gradual increase in the percentage of C-OH corresponding to the hydroxyl group as an oxygen-containing functional group from bare VR (13.4%) to VR/G3 (23.6%). In addition, the phenomenon of an increase of the hydroxyl group was also confirmed from O 1s spectra (see Fig. S2b), where an increased peak related to -OH emitted at 531.5 eV was observed with an increase of amount of the GO in the films. The increased amount of the hydroxyl group on the films can act as active sites directly linked to the  $V_2O_5$ , resulting in an enhancement of  $Li^+$  transport capability to accelerate the EC switching reaction due to the improved wettability with the electrolyte [22,23].

Fig. 4a shows the dependence of the GO on the electrical conductivity of the films. In general, as a low-mobility n-type semiconductor, the  $V_2O_5$  has a poor electrical conductivity ( $10^{-2}$ – $10^{-3}$  S/cm), which of the main factor that contributes to the slow switching speed of the ECDs [24]. Due to the rough film structure with vacant gaps, the electrical conductivity of bare VR was dramatically lower as compared to the corresponding values reported in previous studies. For the VR/GO nanocomposite films, we observed that the electrical conductivity gradually improved with an increase of the amount of the GO, which resulted from the formation of percolated film structure to provide fast electron transport. In addition, the GO can also vary the optical bandgap ( $E_g$ ) of the films determined by extrapolating the linear portion of the curve obtained from the following relationship (Eq. (1)) [25]:

$$(ah\nu)^2 = D(h\nu - E_g)^n \quad (1)$$

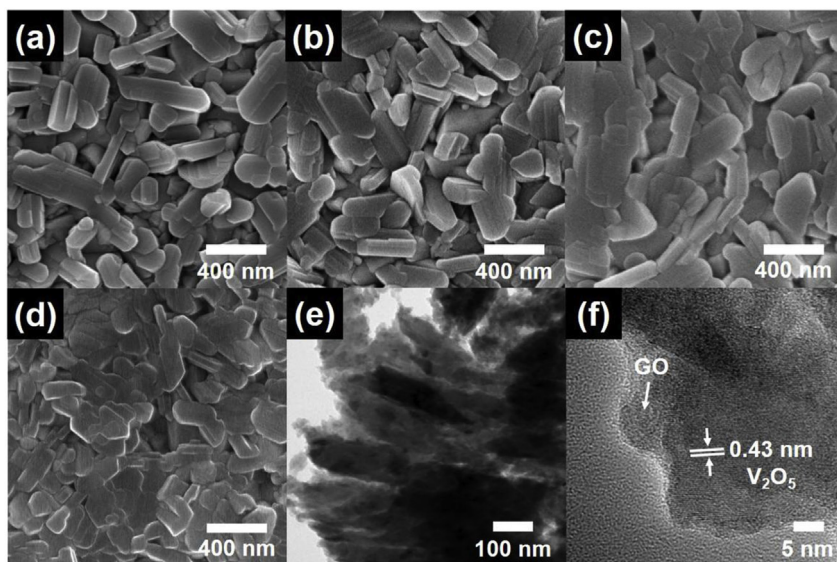


Fig. 1. Top-view FESEM images of (a) bare VR, (b) VR/G1, (c) VR/G2, and (d) VR/G3 and (e) TEM image and (f) enlarged image of VR/G2.

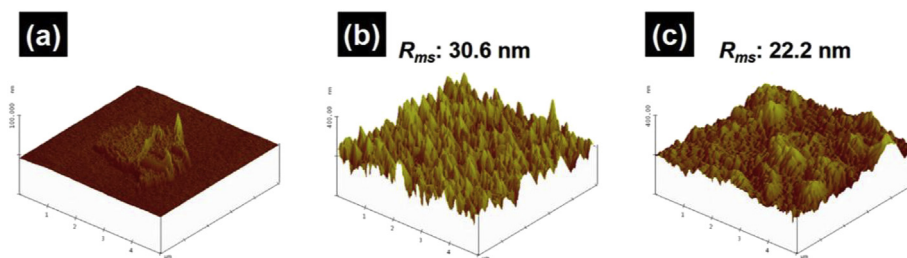


Fig. 2. AFM images of (a) GO, (b) bare VR, and (c) VR/G2.

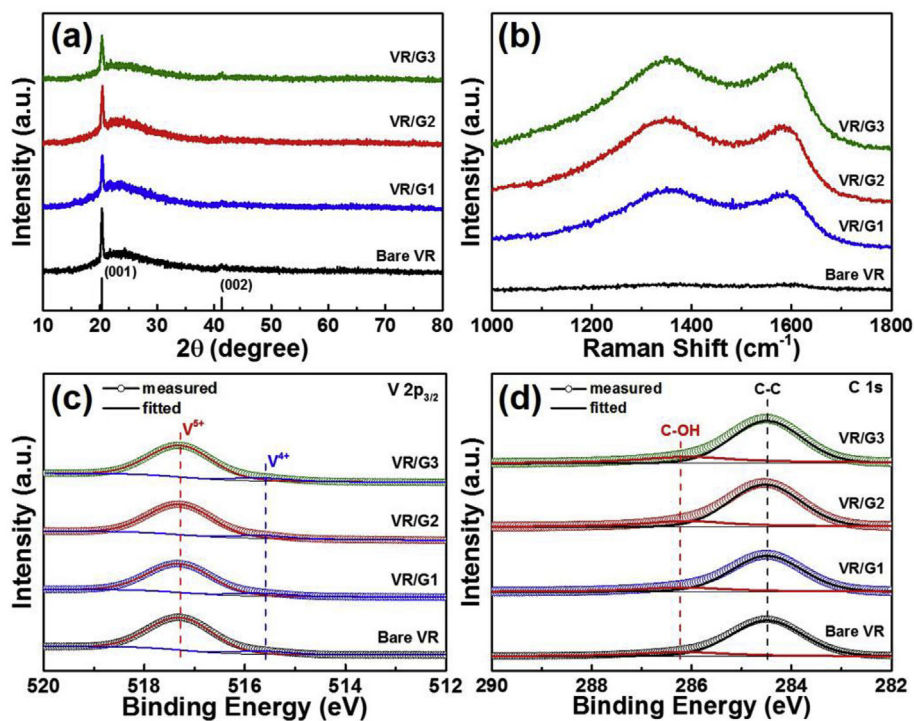


Fig. 3. (a) XRD curve, (b) Raman spectra, and XPS spectra of (c) V 2p<sub>3/2</sub> and (d) C 1s obtained from all films.

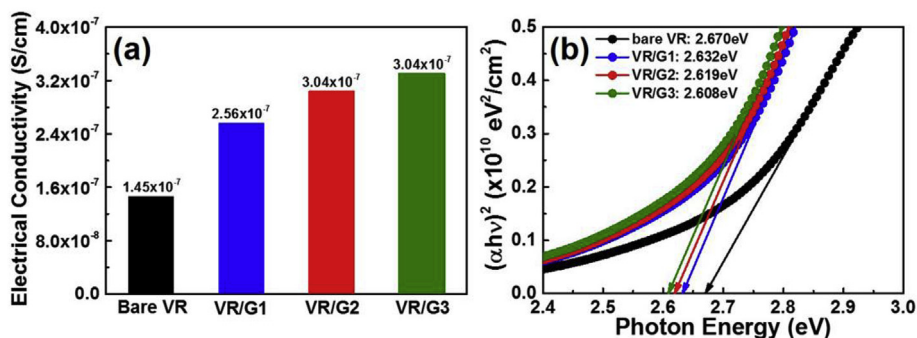


Fig. 4. (a) Electrical conductivity and (b) optical bandgap of all films.

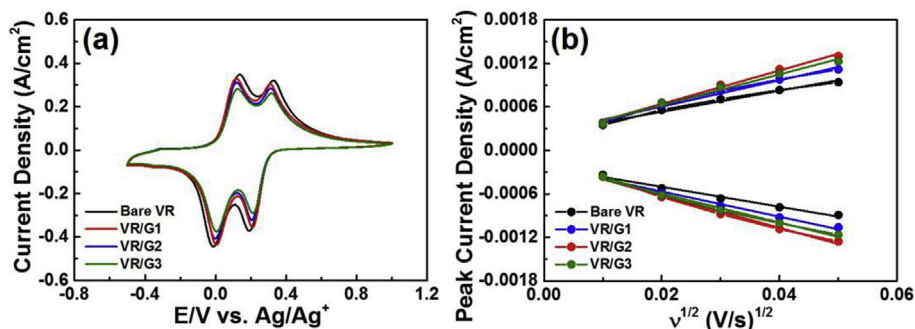


Fig. 5. (a) CV curves measured in the potential range  $-0.5$ – $1.0$  V at scan rate of  $20$  mV/s and (b) peak current density obtained with a function of square root of scan rate.

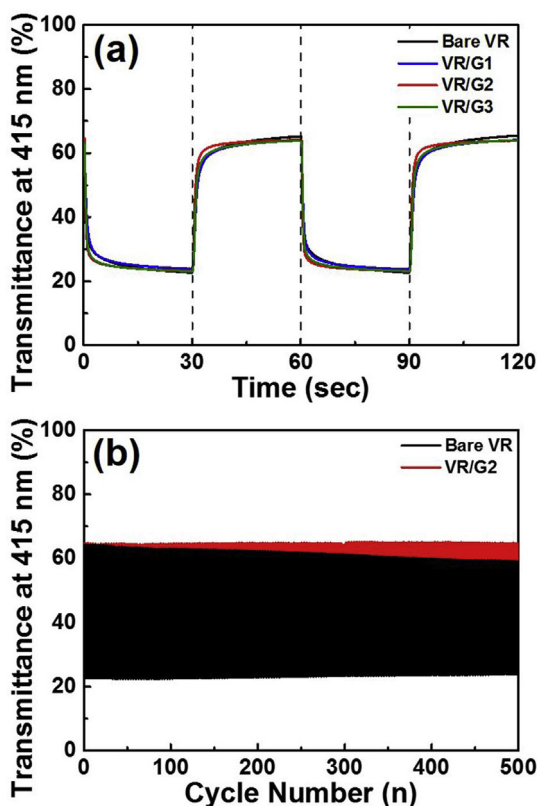


Fig. 6. (a) *in situ* optical transmittance at  $415$  nm with respect to the application of step potential between  $-0.5$  and  $1.0$  V for  $30$  s and (d) variation of transmittance modulation at  $415$  nm as a function of the cycle numbers.

Table 1

Summary of EC performances measured from all films.

	$T_b$ (%)	$T_c$ (%)	Transmittance Modulation (%)	Colouration speed (s)	Bleaching speed (s)
Bare VR	65.28	22.68	42.60	5.6	6.0
VR/G1	64.82	23.83	40.99	3.4	5.2
VR/G2	64.13	23.21	40.92	1.4	2.5
VR/G3	63.94	23.16	40.78	2.3	4.1

where  $h$  is Planck's constant,  $\nu$  is photon frequency, and  $D$  is a constant. As shown in Fig. 4b, due to the relatively lower optical bandgap ( $E_g \approx 0.50$  eV) of the GO as compared to the  $V_2O_5$  ( $E_g \approx 2.67$  eV), narrowing of their optical bandgap was the result of the increased amount of the GO (see Fig. 4b) [26,27]. Therefore, this variation in electrical and optical properties of the films can be directly related to the EC performances, such as transmittance modulation and switching speed.

To characterize the electrochemical behaviour of the films with an amount of the GO, we performed the CV analysis in the potential range from  $-0.5$ – $1.0$  V at the scan rate of  $20$  mV/s using a three-electrode Pt wire as the counter electrode, Ag wire as the reference electrode, and  $1$  M  $LiClO_4$  as the electrolyte (see Fig. 5a). For bare VR, there were multiple steps of redox reactions in the potential range, with the two well-defined reduction peaks centred at  $0.19$  and  $-0.01$  V relative to the  $\alpha/\epsilon$  and  $\epsilon/\delta$  phase transitions, respectively, and the two well-defined oxidation peaks at  $0.14$  and  $0.33$  V relative to the  $\delta/\epsilon$  and  $\epsilon/\alpha$  phase transitions, respectively. These results illustrate the orthorhombic  $V_2O_5$  to reversibly generate multistep  $Li^+$  intercalation/deintercalation processes (see Eq. (2)) [28]:



Interestingly, the gradual potential separation from bare VR to VR/G2, where the reduction and oxidation peaks shifted to higher and lower potentials, respectively, was observed in the CV curves. These

findings suggest that the EC reaction activity of the films improved due to the increased effect of the electrical conductivity. However, for VR/G3, despite the highest electrical conductivity than that of the other films, there was a relaxed potential separation, which may be due to the excessive amount of the GO in the films to reduce the  $V_2O_5$  as the main material for the EC reaction [25]. This can be seen in the  $Li^+$  diffusion coefficient ( $D$ ) of the films obtained from the Randles–Sevcik equation (see Eq. (3)) [26]:

$$J_p = 2.72 \times 10^5 \times D^{1/2} \times C_o \times v^{1/2} \quad (3)$$

where  $J_p$  is the peak current density,  $C_o$  is the concentration of active ions in the solution, and  $v$  is the sweep rate. By considering the CV curves measured at scan rates in the range of 20–100 mV/s, the obtained  $Li^+$  diffusion coefficients in intercalation and deintercalation processes were  $7.16 \times 10^{-10}$  and  $6.35 \times 10^{-10}$  cm<sup>2</sup>/s for bare VR,  $11.14 \times 10^{-10}$  and  $10.60 \times 10^{-10}$  cm<sup>2</sup>/s for VR/G1,  $17.92 \times 10^{-10}$  and  $16.80 \times 10^{-10}$  cm<sup>2</sup>/s for VR/G2, and  $15.28 \times 10^{-10}$  and  $13.39 \times 10^{-10}$  cm<sup>2</sup>/s for VR/G3 (see Fig. 5b). Interestingly, these results show that VR/G2 possesses a higher value of  $Li^+$  diffusion coefficients than those of the other films, which can be ascribed to the optimized amount of the GO in the films to improve the EC reaction activity of the  $V_2O_5$ .

The EC responses the films, which are important performance indicators of the ECDs, were traced by measuring the *in situ* transmittance at 415 nm at the repetitive step potentials of  $-0.5$  V (the bleached state) and  $1.0$  V (the coloured state) for 30 s. The curve (see Fig. 6a) provides information about the transmittance modulation ( $\Delta T = T_b - T_c$ ;  $T_b$  and  $T_c$  which are transmittances in the bleached and coloured states, respectively) and the switching speed (defined as the time to reach 90% of the entire transmittance modulation at 415 nm) of the ECDs are summarized in Table 1. For the transmittance modulation, the slight narrowing from bare VR (42.60%) to VR/G3 (40.78%) was observed, which was due to the inactive EC reaction of the GO in the films [29]. However, the switching speeds gradually accelerated from bare VR (6.0 s for the bleaching speed and 5.6 s for the colouration speed) to VR/G2 (2.5 s for the bleaching speed and 1.4 s for the colouration speed). Such fast switching speeds were induced by the optimized effects of the GO in the films that accelerated the electrical conductivity by the percolated film structure and improved the  $Li^+$  diffusion coefficient by a good wettability of the hydroxyl group. For VR/G3, despite a relative higher amount of the GO, switching speeds were slower than VR/G2 due to the excessive amount of the GO. Furthermore, the cycling retention of the ECDs is a particularly important factor for practical use in industrial applications [30]. Fig. 6b compares changing transmittance modulation between bare VR and VR/G2 during 500 cycling. Compared to bare VR that showed a considerable degradation (17.40%) of the transmittance modulation after 500 cycles, the VR/G2 had a quite good EC cycling retention (94.90% after 500 cycles) with little transmittance modulation (5.10%). This performance improvement is mainly due to the noticeable electrochemical stability of the films resulting from the formation of the percolated film structure by the GO with mechanical stability.

#### 4. Conclusions

In the present study, we successfully developed the VR/GO nanocomposite films to implement stable fast-switching electrochromic performances by optimizing the volume percentage of the GO (0, 1, 2, and 3 wt%). When optimized GO of 2 wt% was used to form the VR films, the elaborate formation of a densely percolated film structure was observed. Owing to the fast electron transport and high wettability of the GO, the proposed method improves both electrical conductivity and ion diffusion coefficient. In addition, this unique film structure can be used to alleviate a physical change in the  $V_2O_5$  lattices by a strong interaction with the GO characterized by a high mechanical stability. As a

result, fast switching speeds (2.5 s for the bleaching speed and 1.4 s for the colouration speed) can be achieved for the VR/GO nanocomposite films fabricated with 2 wt% GO (VR/G2) due to their increased electrical conductivity and ion diffusion coefficient, and the transmittance modulation can retain 94.90% even after 500 cycles, which can be attributed to the percolated film structure formed by the GO. Therefore, we believe that the unique film structure using the  $V_2O_5$  is a promising EC material that ensures highly stable fast-switching electrochromic performance that is required in future-oriented application of the ECDs.

#### Acknowledgement

This work was supported by the National Research Foundation of Korea (NRF) grant funded by the Korea government (MSIT) (No. 2019R1A2C1005836).

#### Appendix A. Supplementary data

Supplementary data to this article can be found online at <https://doi.org/10.1016/j.ceramint.2019.03.148>.

#### References

- [1] K.-H. Kim, B.-R. Koo, H.-J. Ahn, Sheet resistance dependence of fluorine-doped tin oxide films for high-performance electrochromic devices, *Ceram. Int.* 44 (2018) 9408–9413.
- [2] M. Rakibuddin, H. Kim, Synthesis and characterization of facile industrially scalable and cost effective  $WO_3$  micro-nanostructures for electrochromic devices and photocatalyst, *Ceram. Int.* 44 (2018) 16615–16623.
- [3] C.G. Granqvist, M.A. Arvizu, I.B. Pehlivan, H.-Y. Qu, R.-T. Wen, G.A. Niklasson, Electrochromic materials and devices for energy efficiency and human comfort in buildings: a critical review, *Electrochim. Acta* 259 (2018) 1170–1182.
- [4] C.G. Granqvist, Electrochromics for smart windows: oxide-based thin films and devices, *Thin Solid Films* 564 (2014) 1–38.
- [5] B.-R. Koo, K.-H. Kim, H.-J. Ahn, Switching electrochromic performance improvement enabled by highly developed mesopores and oxygen vacancy defects of Fe-doped  $WO_3$  films, *Appl. Surf. Sci.* 453 (2018) 238–244.
- [6] Z. Tong, N. Li, H. Lv, Y. Tian, H. Qu, X. Zhang, J. Zhao, Y. Li, Annealing synthesis of coralline  $V_2O_5$  nanorod architecture for multicolor energy-efficient electrochromic device, *Sol. Energy Mater. Sol. Cells* 146 (2016) 135–143.
- [7] Y. Liu, C. Jia, Z. Wan, X. Weng, J. Xie, L. Deng, Electrochemical and electrochromic properties of novel nanoporous  $NiO/V_2O_5$  hybrid film, *Sol. Energy Mater. Sol. Cells* 132 (2015) 467–475.
- [8] K. Lee, G. Cao, Enhancement of intercalation properties of  $V_2O_5$  film by  $TiO_2$  addition, *J. Phys. Chem. B* 109 (2005) 11880–11885.
- [9] M.M. Margoni, S. Mathuri, K. Ramamurthi, R.R. Babu, V. Ganesh, K. Sethuraman, Hydrothermally grown nano and microstructured  $V_2O_5$  thin films for electrochromic application, *Appl. Surf. Sci.* 449 (2018) 193–202.
- [10] K.-C. Cheng, F.-R. Chen, J.-J. Kai,  $V_2O_5$  nanowires as a functional material for electrochromic device, *Sol. Energy Mater. Sol. Cells* 90 (2006) 1156–1165.
- [11] R. Narayanan, A. Dewana, D. Chakraborty, Complimentary effects of annealing temperature on optimal tuning of functionalized carbon- $V_2O_5$  hybrid nanobelts for targeted dual applications in electrochromic and supercapacitor devices, *RSC Adv.* 8 (2018) 8596–8606.
- [12] C.E. Patil, P.R. Jadhav, N.L. Tarwal, H.P. Deshmukh, M.M. Karanjkar, P.S. Patil, Electrochromic performance of mixed  $V_2O_5$ - $MoO_3$  thin films synthesized by pulsed spray pyrolysis technique, *Mater. Chem. Phys.* 126 (2011) 711–716.
- [13] C.F. Azevedo, R.D.C. Balboni, C.M. Chohant, E.A. Moura, R.M.J. Lemos, A. Pawlicka, A. Gündel, W.H. Flores, M. Pereira, C.O. Avellaneda, New thin films of NiO doped with  $V_2O_5$  for electrochromic applications, *J. Phys. Chem. Solids* 110 (2017) 30–35.
- [14] T. Ivanova, A. Harizanova, Electrochromic investigation of sol-gel-derived thin films of  $TiO_2$ - $V_2O_5$  Mater, *Res. Bull.* 40 (2005) 411–419.
- [15] G. Goncalves, P.A.A.P. Marques, C.M. Granadeiro, H.I.S. Nogueira, M.K. Singh, J. Grácio, Surface modification of graphene nanosheets with gold nanoparticles: the role of oxygen moieties at graphene surface on gold nucleation and growth, *Chem. Mater.* 21 (2009) 4796–4802.
- [16] Y. Li, X. Lv, J. Lu, J. Li, Preparation of  $SnO_2$ -nanocrystal/graphene-nanosheets composites and their lithium storage ability, *J. Phys. Chem. C* 114 (2010) 21770–21774.
- [17] A. Pan, J.-G. Zhang, Z. Nie, G. Cao, B.W. Arey, G. Li, S.-Q. Liang, J. Liu, Facile synthesized nanorod structured vanadium pentoxide for high-rate lithium batteries, *J. Mater. Chem.* 20 (2010) 9193–9199.
- [18] M. Li, G. Sun, P. Yin, C. Ruan, K. Ai, Controlling the formation of rodlike  $V_2O_5$  nanocrystals on reduced graphene oxide for high-performance supercapacitors, *ACS Appl. Mater. Interfaces* 5 (2013) 11462–11470.
- [19] C. Han, M. Yan, L. Mai, X. Tian, L. Xu, X. Xu, Q. An, Y. Zhao, X. Ma, J. Xie,  $V_2O_5$  quantum dots/graphene hybrid nanocomposite with stable cyclability for advanced lithium batteries, *Nanomater. Energy* 2 (2013) 916–922.
- [20] K.S. Kim, Y. Zhao, H. Jang, S.Y. Lee, J.M. Kim, K.S. Kim, J.-H. Ahn, P. Kim, J.-

- Y. Choi, B.H. Hong, Large-scale pattern growth of graphene films for stretchable transparent electrodes, *Nature* 457 (2009) 706–710.
- [21] B. Sen, S. Kuzua, E. Demir, S. Akocak, F. Sen, Monodisperse palladium-nickel alloy nanoparticles assembled on graphene oxide with the high catalytic activity and reusability in the dehydrogenation of dimethylamine-borane, *Int. J. Hydrogen Energy* 42 (2017) 23276–23283.
- [22] J. Fan, S. Liu, J. Yu, Enhanced photovoltaic performance of dye-sensitized solar cells based on TiO<sub>2</sub> nanosheets/graphene composite films, *J. Mater. Chem.* 22 (2012) 17027–17036.
- [23] D. Wan, C. Yang, T. Lin, Y. Tang, M. Zhou, Y. Zhong, F. Huang, J. Lin, Low-temperature aluminum reduction of graphene oxide, electrical properties, surface wettability, and energy storage applications, *ACS Nano* 6 (2012) 9068–9078.
- [24] J.C. Badot, A. Mantoux, N. Baffier, O. Dubrunfaut, D. Lincot, Electrical properties of V<sub>2</sub>O<sub>5</sub> thin films obtained by atomic layer deposition (ALD), *J. Mater. Chem.* 14 (2004) 3411–3415.
- [25] B.-R. Koo, D.-H. Oh, H.-J. Ahn, Influence of Nb-doped TiO<sub>2</sub> blocking layers as a cascading band structure for enhanced photovoltaic properties, *Appl. Surf. Sci.* 433 (2018) 27–34.
- [26] H. Chang, Z. Sun, Q. Yuan, F. Ding, X. Tao, F. Yan, Z. Zheng, Thin film field-effect phototransistors from bandgap-tunable, solution-processed, few-layer reduced graphene oxide films, *Adv. Mater.* 22 (2010) 4872–4876.
- [27] R. Saravanan, S. Joicy, V.K. Gupta, V. Narayanan, A. Stephen, Visible light induced degradation of methylene blue using CeO<sub>2</sub>/V<sub>2</sub>O<sub>5</sub> and CeO<sub>2</sub>/CuO catalysts, *Mater. Sci. Eng. C* 33 (2013) 4725–4731.
- [28] W. He, Y. Liu, Z. Wan, C. Jia, Electrodeposition of V<sub>2</sub>O<sub>5</sub> on TiO<sub>2</sub> nanorod arrays and their electrochromic properties, *RSC Adv.* 6 (2016) 68997–69006.
- [29] A.R. Park, J.S. Kim, K.S. Kim, K. Zhang, J. Park, J.H. Park, J.K. Lee, P.J. Yoo, Si–Mn/Reduced graphene oxide nanocomposite anodes with enhanced capacity and stability for lithium-ion batteries, *Appl. Mater. Interfaces* 6 (2014) 1702–1708.
- [30] B.-R. Koo, H.-J. Ahn, Fast-switching electrochromic properties of mesoporous WO<sub>3</sub> films with oxygen vacancy defects, *Nanoscale* 9 (2017) 17788–17793.